

See discussions, stats, and author profiles for this publication at: <https://www.researchgate.net/publication/299286176>

The effect of infill walls on the seismic behavior of boundary columns in RC frames

Article in *Earthquakes and Structures* · March 2016

DOI: 10.12989/eas.2016.10.3.539

CITATIONS

6

READS

292

5 authors, including:



Aksel Fenerci

Norwegian University of Science and Technology

24 PUBLICATIONS 227 CITATIONS

SEE PROFILE



Baris Binici

Middle East Technical University

116 PUBLICATIONS 1,525 CITATIONS

SEE PROFILE



Pourang Ezzatfar

8 PUBLICATIONS 33 CITATIONS

SEE PROFILE



Erdem Canbay

Middle East Technical University

58 PUBLICATIONS 606 CITATIONS

SEE PROFILE

Some of the authors of this publication are also working on these related projects:



Punching [View project](#)



HSC Research [View project](#)

The effect of infill walls on the seismic behavior of boundary columns in RC frames

Aksel Fenerci¹, Baris Binici², Pourang Ezzatfar³, Erdem Canbay² and Guney Ozcebe³

¹Department of Structural Eng., Norwegian Univ. of Science and Tech., 7491, Trondheim, Norway

²Department of Civil Engineering, Middle East Technical University, 06800 Ankara, Turkey

³Department of Civil Engineering, TED University, 06420 Ankara, Turkey

(Received , Revised , Accepted)

Abstract. The seismic behavior of a ½ scaled, three-story three-bay RC frame with masonry infill walls was studied experimentally and numerically. Pseudo-dynamic test results showed that despite following the column design provisions of modern seismic codes and neglecting the presence of infill walls, shear induced damage is unavoidable in the boundary columns. A finite element model was validated by using the results of available one-story one-bay frame tests in the literature. Simulations of the examined test frame demonstrated that boundary columns are subjected to shear demands in excess of their shear capacity. Seismic assessment of the test frame was conducted by using ASCE/SEI 41-06 (2006) guidelines and the obtained results were compared with the damage observed during experiment. ASCE/SEI 41-06 method for the assessment of boundary columns was found unsatisfactory in estimating the observed damage. Damage estimations were improved when the strain limits were used within the plastic hinge zone instead of column full height.

Keywords: pseudo-dynamic testing; masonry infill wall; finite element method; seismic assessment

1. Introduction

Reinforced concrete (RC) frames with unreinforced masonry (URM) infill walls constitute a significant portion of the building stock throughout the world. Infill walls in these buildings are generally considered as non-structural elements. Observations after several earthquakes revealed that infill walls may significantly alter the response of adjacent columns (Binici *et al.* 2012) Studies in the literature point out that infill walls increase lateral stiffness and strength of a frame subjected to seismic excitations under low to moderate seismic demands. Under strong seismic excitations, sudden failure of masonry infill walls may accelerate the damage in the structural elements (Fiorato *et al.* 1970, Bertero and Brokken 1983, Mehrabi *et al.* 1994). An important risk posed by the infill walls is due to the shear demands on columns adjacent to the masonry infill walls, named hereafter as boundary columns.

Over the past few decades, the interaction of the infill walls with their bounding frames was investigated by a number of researchers. Fiorato *et al.* (1970) conducted a study on the effects of masonry infilled RC frames and tested eight one-story one-bay, thirteen five-story one-bay and six

* Corresponding author, Professor, E-mail: binici@metu.edu.tr

two-story three-bay 1/8 scale RC frames which had masonry infill walls. The comprehensive study revealed that the presence of infill walls increase the lateral stiffness and strength of the frames significantly. Mehrabi *et al.* (1994) carried out monotonic and cyclic experiments on fourteen 1/2 scale concrete block masonry infilled RC frames consisted of both code compliant and deficient RC frames. In their study, the behavior of specimens with different frame to infill wall stiffness and strength ratios were examined. They concluded that shear failure of boundary columns occur in case of weak frames with strong infill walls. Marjani (1997) investigated the behavior of plastered and non-plastered brick infilled reinforced concrete frames under reversed cyclic loading and conducted experiments on six two-story one-bay frames. The strength increase was about 240% for the non-plastered specimens and 300% for the plastered ones compared to the bare frame. Mosalam *et al.* (1998) tested a multi-story multi-bay concrete block masonry infilled steel frame having openings with pseudo-dynamic (PsD) experimentation technique. Fardis *et al.* (1999) conducted shake table tests on a two-story, single-bay three-dimensional RC frame and studied the effects of plan irregularities caused by non-uniform distribution of the masonry infill walls. Hashemi and Mosalam (2007) conducted both shake table and PsD tests on two separate 3/4 scale one-story one-bay RC frames to investigate in and out-of-plane behavior of the infill walls. More recently, Kurt *et al.* (2011) used PsD method for testing a 1/2 scale two-story three-bay RC frame and evaluated its seismic performance. Aforementioned studies provide an essential understanding of the frame-infill wall interaction reaching the conclusion that the frame response can be altered significantly due to the infill wall-frame interaction. In most cases, the frame behaves as a monolithic load-carrying system at low deformation demands. As the lateral deformations increase on a building with a frame system having infill walls, separation of the infill wall from the bounding frame occurs leading to the formation of a compression strut mechanism along the other diagonal (Fig. 1). In the above-mentioned studies, it was observed that depending on the strength and stiffness properties of the infill wall and its bounding frame, the compression strut either contributes to the load carrying system or causes brittle shear failure of the boundary columns. However, the adequateness of the seismic design practice was not assessed critically and the findings were not codified.

In parallel to this design oriented look at the problem, many other researchers focused on simulating the behavior of masonry infill walls inside building frames, realizing the importance of their contribution to earthquake response. Various degrees of sophistication were employed in the infill models from macro models based on strut models (Klinger and Bertero 1976, Mainstone 1971, El-Dakhkhni *et al.* 2003), to more complicated finite element (FE) models with smeared crack (Mosalam *et al.* 1998, Hashemi and Mosalam 2007) and discrete crack approaches Mehrabi and Shing 1997, Stavridis and Shing 2010). Among those modeling options, continuum modeling with smeared crack approach is preferred in this study. Smeared crack models are well tested, stable, established and require relatively less parameters for calibration compared to discrete models (for example Vecchio and Collins 1993, Selby and Vecchio 1993). They are superior to strut models as they allow observing the behavior of the boundary columns and the forces acting on them. They are computationally less expensive and more practical compared to the discrete crack approach where every interface should be modeled separately. In the above-mentioned studies, although the analytical results match the experimental findings with good accuracy, the calibrations of models were usually conducted for a limited amount of test results and unfortunately could not be generalized to estimate the performance of masonry infill wall behavior in RC frames. In this regard, further experimental data and numerical simulations are important and necessary to better estimate the forces transferred from the infill walls to the boundary frame members, which sets forth the key objective for this study.

In the performance assessment guidelines of ASCE/SEI 41-06 (2006), the columns adjacent to infill walls are considered as tension and compression ties. The average axial strain demands along the height of the columns rather than plastic hinge rotations are considered in the assessment. Table 1 presents the axial strain limits given in ASCE/SEI 41-06 for the seismic assessment of boundary columns in infilled frames. The guidelines also require the shear strength of columns to be greater than the shear force demand, which can be calculated from the horizontal component of the strut force or the shear force due to the reduced length (l_{ceff}) of the column (Fig. 1). However, which force among these two options to consider remains unclear. Eurocode 8 (2004), on the other hand, requires the boundary columns to have transverse reinforcement details similar to the end confining regions throughout the column length in design. In addition, the shear strength of the boundary columns is required to exceed the smaller of the horizontal component of the strut force and the shear force due to the reduced length (l_{ceff}) of the column (Fig. 1). The selection of the shear force demand from the smaller of the two forces described above appears to be in conflict with intuition. Eurocode 8 seems to be the only guideline providing additional steel detailing regulations for the design of boundary columns.

The purpose of the current study is to investigate the RC frame-infill wall interaction by employing the pseudo-dynamic test results. The test frame was designed according to the Turkish Earthquake Code (TEC, 2007) which includes all the principles of modern earthquake resistant design practice. Pseudo-dynamic testing was conducted under three levels of ground motion. A nonlinear continuum finite element (FE) model was developed and the ability of the model to estimate the local and global engineering demand parameters was investigated. Afterwards, the results of the nonlinear analysis were employed to deduce the force distributions on the boundary columns, which cannot be obtained from the experiments. Finally, the accuracy of the ASCE/SEI-41-06 guidelines for the assessment of infill walls and boundary columns in estimating the observed damage was critically evaluated.

Table 1 Numerical acceptance criteria for columns adjacent to infill walls (ASCE/SEI 41-06 2006)

Acceptance Criteria	Total Strain		
	Performance Level		
	IO	LS	CP
Conditions			
i. Columns modeled as compression chords			
Columns confined along entire length	0.003	0.015	0.02
All other cases	0.002	0.002	0.003
ii. Columns modeled as tension chords			
Columns with well-confined splices, or no splices	0.01	0.03	0.04
All other cases	See the document		

2. Experimental program

2.1 Specimens and testing

The 1/2 scaled three-story three-bay reinforced concrete frame with masonry infill walls at its central bay (Fig. 2) was selected from a typical interior frame of an RC prototype building. The building was designed according to the TEC provisions. Gravity loads were applied on the flanged beams

with steel blocks to represent the dead and live loads (Fig. 2). All columns had rectangular sections, $150 \text{ mm} \times 200 \text{ mm}$ in size. They were reinforced with 8-10 mm diameter longitudinal bars, which correspond to a reinforcement ratio of 2.3 percent (Fig. 3). The first story columns were named and will be referred hereafter as column 101,102,103 and 104 as shown in Fig. 2. 4 mm diameter plain bars were used to fabricate the stirrups and the ties. They were also used as longitudinal reinforcement within the flanges of the beams. The end zones of both beams and columns were properly confined (Fig. 3). Infill walls were constructed according to the common construction practice by using hollow clay bricks, which had dimensions of $95 \text{ mm} \times 100 \text{ mm} \times 190 \text{ mm}$ (Fig. 3). The brick units were laid so that holes were in the vertical direction. Thickness of the applied plaster on the infill wall surfaces on both sides was approximately 10 mm. Material properties were obtained from material tests and presented in the numerical simulations section.

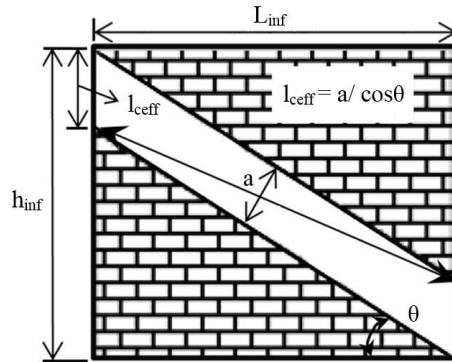


Fig. 1 Forces transferred from infill walls to boundary columns in seismic codes

Instrumentation consisted of Linear Variable Differential Transformers (LVDTs) which were placed at each story level and at the member ends of the first story columns to measure the story deformations and member end rotations. Diagonal infill wall displacements were measured with dial gages placed at the first story infill diagonal. Base moments, shear and axial forces were obtained by the three-component force transducers (Canbay *et al.* 2004) attached at the bottom of the exterior columns (Fig. 2). More detailed information about the test setup and instrumentation can be found in Sucuoglu *et al.* 2013.

The three degree-of-freedom system was tested using the continuous PsD method (Molina *et al.* 1999a). Using the ground acceleration record, the equation of motion for the structure was solved numerically with an explicit time integration scheme and the calculated displacement demands were applied to the structure with the help of the hydraulic actuators. Mass matrix used was diagonal and consistent with the story masses ($m_1 = 11426 \text{ kg}$, $m_2 = 11426 \text{ kg}$, $m_3 = 7925 \text{ kg}$) of the scaled structure. Three synthetic ground acceleration records were generated and scaled to match the site-specific spectra of the Duzce region where the disastrous Duzce earthquake took place in 1999 (Erdik 2000). D1 and D2 ground motions represent 50% and 10% probability of being exceeded in 50 years for Z1 type of soil respectively, whereas D4 ground motion represents 10% probability of being exceeded in 50 years for Z3 type of soil. Here, Z1 type soil corresponds to rock where Z3 corresponds to stiff clay according to TEC (2007). In the experiments, different soil types were used to observe the possible effects of soil amplification on reinforced concrete frames experimentally. Original ground motions shown in Fig. 4 were compressed in the time domain by the factor of $1/\sqrt{2}$, to be compatible with the similitude law.

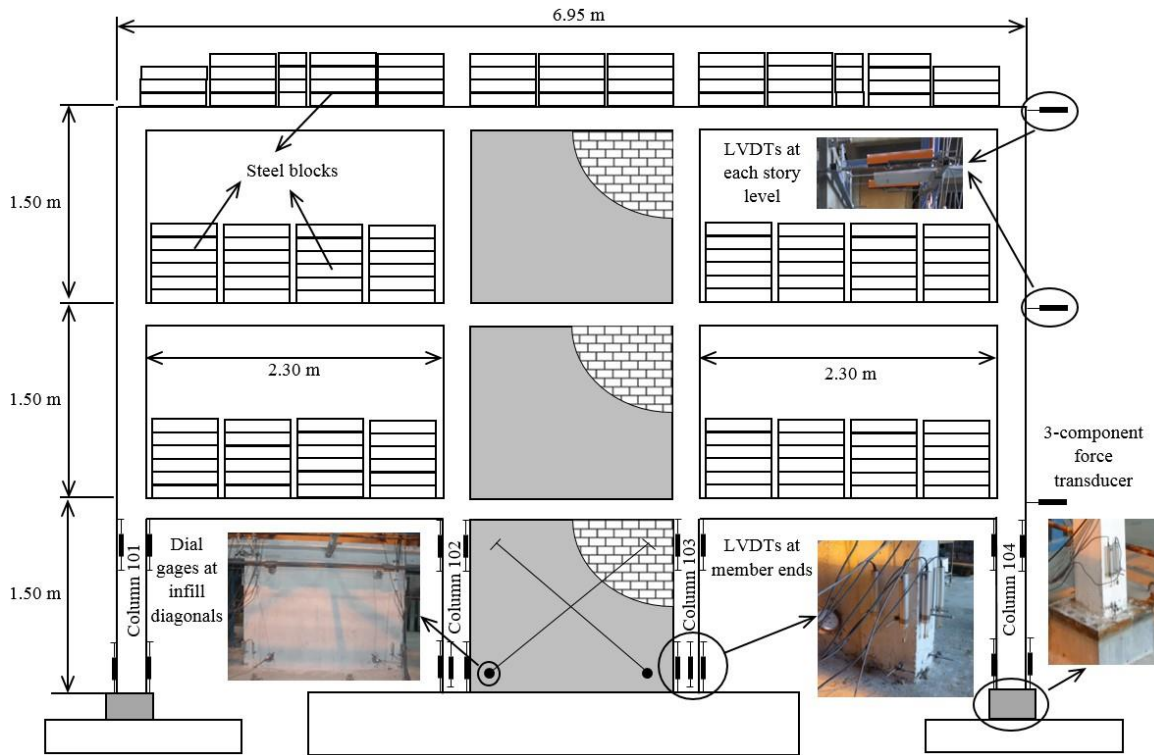


Fig. 2 Details of the test frame and instrumentation

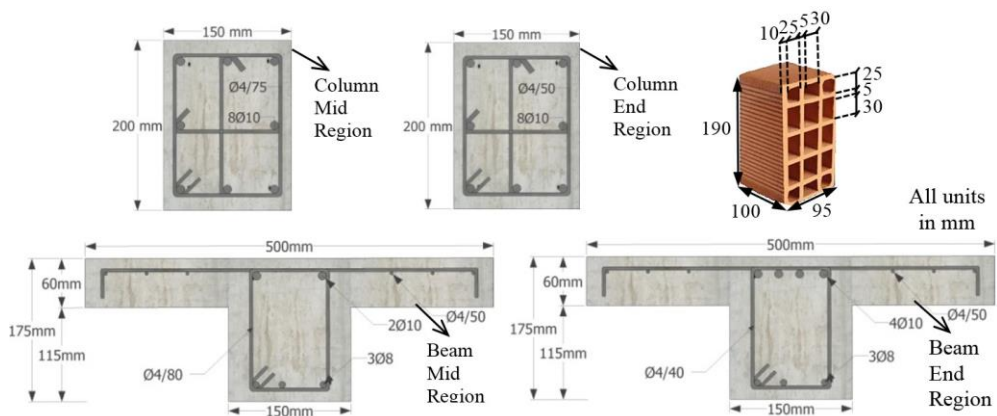


Fig. 3 Section properties

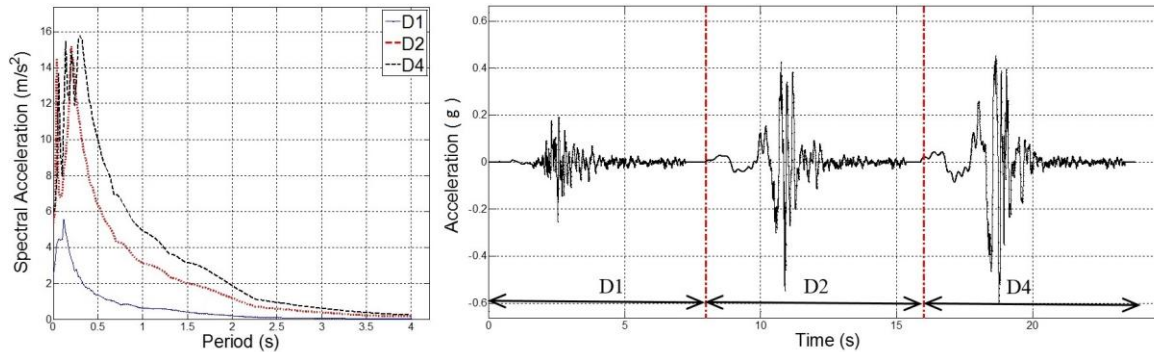


Fig. 4 Ground motions used in experiments

2.2 Results

The interstory drift ratios versus time plots of all three stories are given in Fig. 5. On the same figure, the observed damages in different members of the test structure are also shown. For the D1 ground motion, the test frame did not exhibit any nonlinear response under relatively small displacement demands. The second ground motion, D2 resulted in interface cracks at the frame-infill wall boundaries. Horizontal sliding cracks at the first story infill wall and cracks at the first story boundary columns due to frame-infill wall interaction were also observed. Maximum interstory drift ratio of the first story at the end of D2 ground motion was about 0.7 percent at a roof displacement of 28 mm. D4 ground motion caused significant damage on the test frame, resulting in widening of the existing cracks in the first story infill wall, which resulted the test frame to experience large first story drifts.

Base shear versus roof displacement responses for the D1, D2 and D4 ground motions are presented in Fig. 6. In the same figure, story shear versus interstory drift ratio plots for each floor are also given. From the load displacement curves, it is observed that significant stiffness deterioration occurred during D4 ground motion. However, lateral strength drop was quite marginal.

Flexural and shear cracks on boundary columns were also observed (Fig. 5). In the second story, interface cracks at the frame-infill wall boundary and a diagonal crack at the URM infill wall were developed. The hysteretic load deformation response was severely pinched due to the opening and closing of cracks in both infill walls (Fig. 6). For D4 ground motion, the maximum interstory drift ratio of the first floor was about 2.0 percent, which resulted in 43 mm roof displacement (Fig. 6). Maximum base shear demand measured during experiment was 200 kN. Identification of the time dependent vibration periods of the test frame was made using the procedure proposed by Molina *et al.* (1999b) and the first mode periods of the test frame were calculated as 0.17, 0.21 and 0.45 seconds at the beginning of D1, D2 and D4 ground motions, respectively. The computed fundamental period of the model was about 0.2 seconds, which matched well with identified values at the beginning of D1 and D2 motions. The first mode period at the end of the experiment was calculated as 0.53 seconds. Eigenvalue analysis on the damaged specimen could not be conducted due to the limitations of the algorithm in DIANA (2008); hence, a direct comparison of periods could not be made for the damaged specimen.

There are a number of studies examining the behavior of infilled frame behavior by employing a one-bay one story test by applying increasing cyclic displacement excursions (for example Mehrabi 1994, Kakaletsis and Karayannis 2007, 2009). It is felt important to mention here some of the key

differences observed in the tests presented herein with the results of one-bay one-story infilled frame tests in the literature. By conducting a three-bay three-story system test with actual ground motion input, one can obtain more realistic estimations of demand parameters including story deformations, joint and plastic hinge rotations. The load-deformation response measurements in the three-story three-bay specimen suggest the presence of higher mode effects (irregular nature of the curves), which could not be observed in cyclic one-bay one-story tests. With a multistory test setup, the observed damage in the beam-column connections is usually less than that observed in one-bay one-story tests due to the absence of members joining at the joints. Furthermore, in a three-story test specimen, soft-story formation (as described in Favvata et. al. 2013) due to the infill wall damage could be observed. Multi-story multi-bay testing by no means can lessen what is learnt from single story frame tests, but it can perhaps augment the knowledge by providing a wider perspective on damage sequence and redistribution.

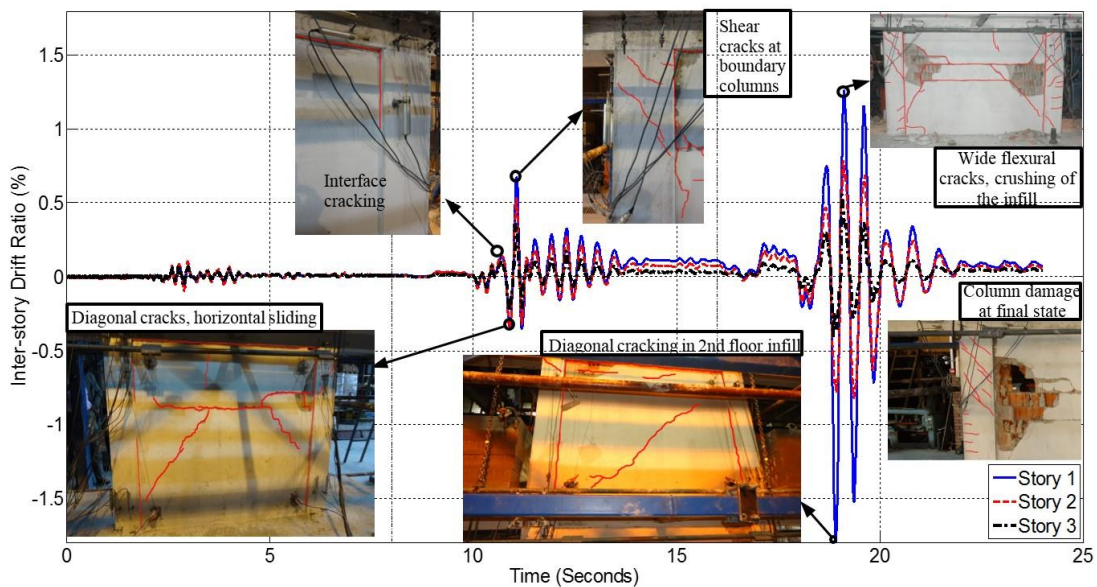


Fig. 5 Interstory drift ratio response along with damage patterns

3. Numerical simulations

3.1 Modeling

A continuum plane stress finite element model of the test frame was constructed using DIANA (2008). The reinforced concrete frame was modeled with 8-node quadrilateral iso-parametric elements, which were based on quadratic interpolation and integrated numerically by a 2×2 Gauss integration method. Total strain rotating crack model was used to simulate the nonlinear behavior of reinforced concrete (Selby and Vecchio 1993). The concrete material model describes both the compressive and tensile behavior by stress-strain relationships in the principle directions. Concrete uniaxial behavior was modeled as a linearly elastic and brittle material response in tension and parabolic response (Fig. 7) based on fracture energy (Feenstra 1993) in compression. The embedded reinforcement approach (DIANA 2008) assumes that the reinforcement elements do not have their own degrees of freedom but can add stiffness to the mother elements in the finite

element model. Reinforcing bars were modeled at their exact geometric locations in the finite element mesh. Perfect bond was assumed between concrete and steel. For steel, a bilinear kinematic hardening stress-strain relationship was used to model both uniaxial tension and compression behavior.

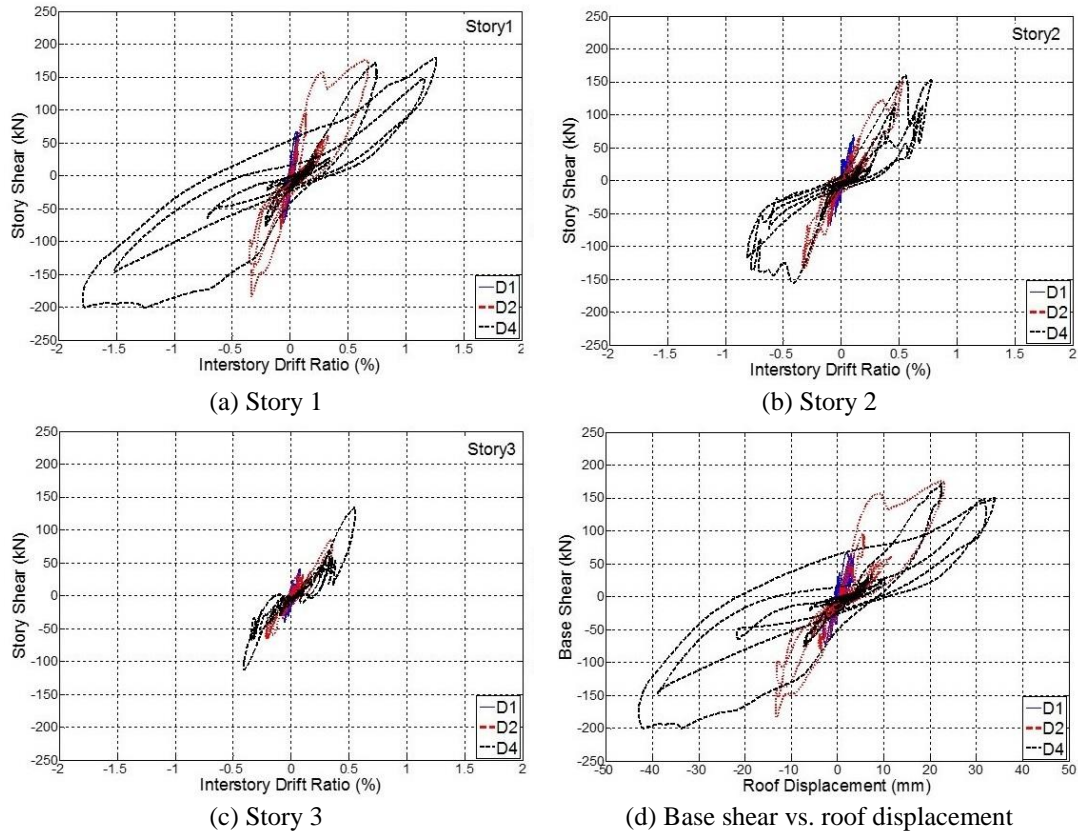


Fig. 6 Force - deformation response

The frame-infill wall interfaces were modeled using 6-node interface elements with a Coulomb friction criterion (DIANA 2008). Due to lack of experimental data on the frame-wall interfaces, average values were used from Mehrabi *et al.* (1994) as model parameters. Linear normal and tangential stiffnesses of interfaces were assumed equal to each other (Fig. 8). The normal and tangential stiffnesses define the relationship between traction and elastic displacement vectors in normal and tangential directions to the interface direction. Cohesion and friction angle were assumed to be 0.5 MPa and 26° , respectively. Zero dilatancy angle was assumed. Cohesion and friction hardening rules were ignored and a non-associated flow rule was assumed with a gap criterion, which was defined with a low tensile strength (0.1 MPa). This model assumed that a gap forms if the traction exceeds the assigned tensile strength.

The masonry wall was modeled as a continuum similar to the RC frame. URM infill wall was meshed using 8-node quadrilateral iso-parametric plane-stress finite elements. The infill wall elements were then assigned a rotating crack constitutive model by using the formulation of Selby

and Vecchio (1993). Such an approach for masonry was previously employed by Hashemi and Mosalam (2007) and Van Noort (2012), successfully. Uniaxial stress-strain behavior of the infill wall was modeled with a parabolic model in compression (Feenstra 1993). For the tension behavior, a linear elastic behavior followed by a loss of strength region to simulate cracking was employed. For the lateral cracking, model proposed by Vecchio and Collins (1993) based on experimental data was used for both concrete and masonry which modifies the uniaxial stress-strain relationship depending on the tensile strain along the transverse direction. The modification is done simply by reducing the ultimate stress and strain by the factor given in Equation 1 upon cracking. The reduction factor can be calculated using:

$$\beta = \frac{1}{1 + 0.27 \left(\frac{\varepsilon_{lat}}{\varepsilon_0} - 0.37 \right)} \quad (1)$$

$$\varepsilon_{lat} = \sqrt{\varepsilon_1^2 + \varepsilon_2^2} \quad (2)$$

where ε_1 and ε_2 refers to the principal strains in two lateral directions and ε_0 refers to the strain corresponding to ultimate stress in the unmodified stress-strain curve.

The gravity load applied on the beams of the test frame was simulated by uniformly distributed loads on the beams. Story masses were lumped at the nodes and they were consistent with the mass matrix, which was used in the PsD testing protocol. Rayleigh damping was used to simulate the damping effects. The final finite element mesh composed of 4,917 plane stress elements and 342 interface elements. A summary of the modeling strategy is presented in Fig. 7. In the figure, c and ϕ represent the cohesion and the friction angle where t_n and t_t represent the normal and tangential tractions, respectively. Material properties were obtained from uniaxial compression tests on concrete cylinders, prism tests on masonry and mortar assemblages and uniaxial tension tests on steel reinforcing bars. The tensile strength of the concrete was calculated according to TEC (2007). For masonry, 3% of the compressive strength was taken as the tensile strength following the suggestion of Hashemi and Mosalam (2007). Fracture energy for concrete was calculated according to Feenstra (1993). All the material properties used in the simulations are given in Table 2.

3.2 Validation

The capability of the proposed FE model to simulate the highly nonlinear behavior of the frame-infill wall interaction and the resulting failure modes were investigated using the experiments conducted by Mehrabi *et al.* (1994). Mehrabi tested ten single-story single-bay RC frames with different infill wall and frame characteristics. The main parameter of the test was the infill wall to frame strength ratio. Characteristics and material properties of each test frame can be found in Mehrabi *et al.* (1994). The strategy described in the previous section was employed here to validate the model. Here, material properties of the wall medium were obtained from the prism tests on masonry assemblages (Mehrabi *et al.* 1994). In addition, the elastic stiffness properties of the interfaces were obtained from joint direct shear tests, which were conducted on mortar specimens (Mehrabi *et al.* 1994). The validation of the cyclic joint shear tests with the interface model is shown in Fig. 8.

Inelastic pushover analyses were carried out for each test frame tested by Mehrabi *et al.* (1994). The finite element mesh used in the simulations is presented in Fig. 9. The results of the analyses are presented along with the experimental results (Fig. 10). The comparisons of the load-displacement curves obtained from simulations and experiments show that the analyses succeeded in estimating the capacity of the URM infilled frames with a maximum error of 20%. The post-peak response was on the other hand, not represented well for some of the simulations, which is attributed to not matching the local failure modes in the test exactly. In other words, step-wise cracking and sliding across masonry interfaces could not be simulated very accurately with a smeared crack model, as it is not directed towards a collapse type simulation. However, in a global sense, one can argue the general engineering agreement between experimental and simulation results. It is important to mention that at a drift level of 2 percent, which is the maximum level of expected deformation demand for a well-designed structure, the capacity estimations had an error of at most 20%. For the majority of the frames, the lateral stiffness estimations were in reasonable agreement with the experimental values whereas in some cases (specimens 3, 4 and 7) premature cracking in the analysis resulted in early softening, which could not be simulated well.

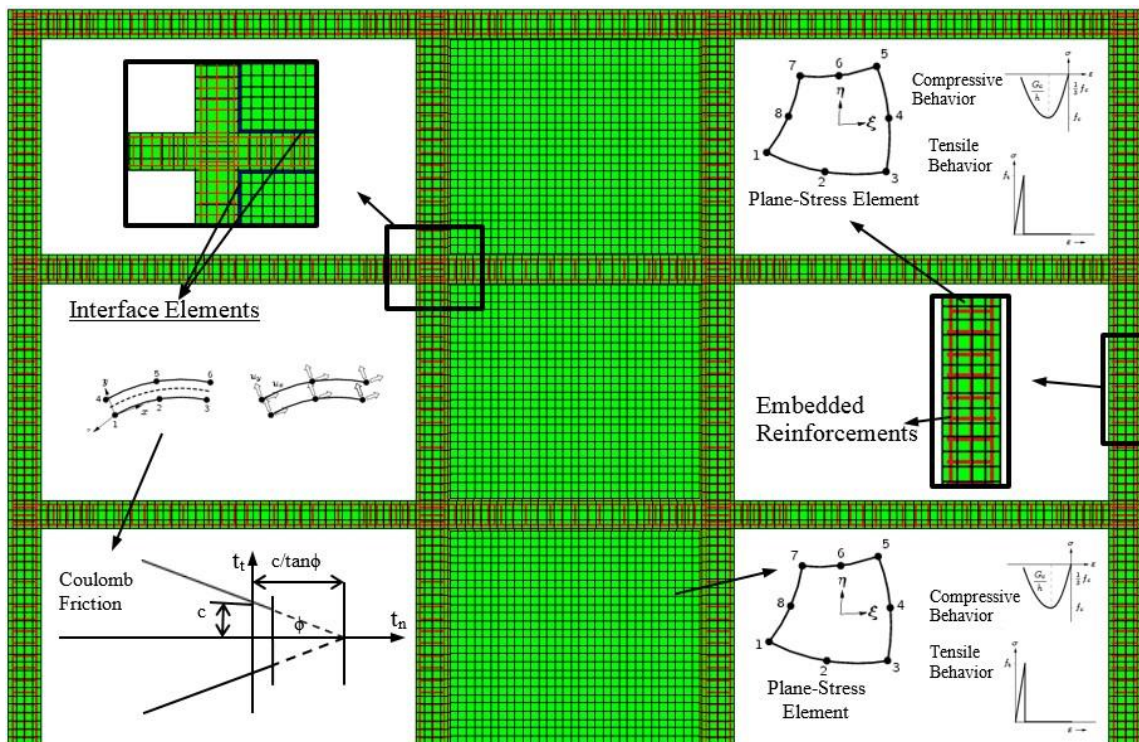
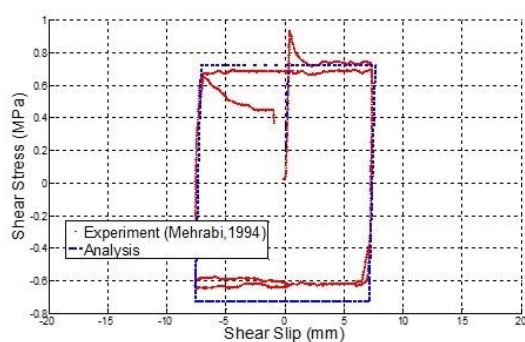
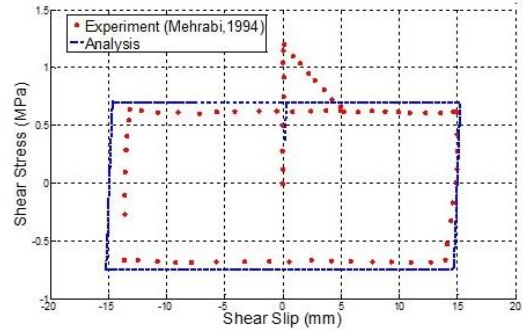


Fig. 7 Modeling Strategy



(a) Hollow brick

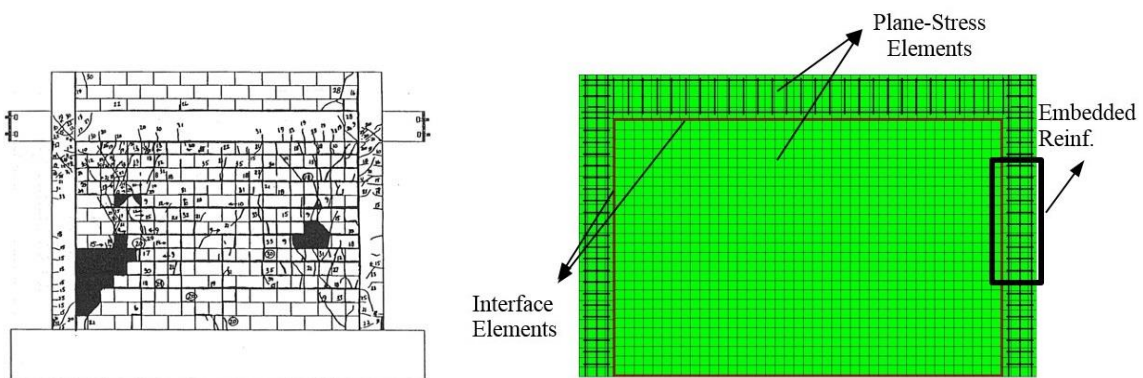


(b) Solid brick

Fig. 8 Results of cyclic joint direct shear tests (Mehrabi *et al.* 1994)

Table 2 Material properties used in numerical simulations

Wall Medium	Mortar (Interfaces)		
Elastic Modulus E_c (MPa)	850	Normal Stiffness K_{nn} (N/m ³)	8.5×10^{11}
Compressive Strength f_c (MPa)	8.5	Tangential Stiffness K_{tt} (N/m ³)	8.5×10^{11}
Tensile Strength f_{ct} (MPa)	0.25	Cohesion c (MPa)	0.5
Compressive Fracture Energy, G_c (N.m/m ²)	200	Friction Angle ($\tan\phi$)	0.5
	Reinforcing Steel ($E = 200,000$ MPa)		
Concrete	Reinforcing Bar	Yield Strength (MPa)	Ultimate Strength (MPa)
Elastic Modulus E_c (MPa)	21,00		
Compressive Strength f_c (MPa)	19.6	4 mm plain bars	240
Tensile Strength f_{ct} (MPa)	1.55	8 mm deformed	450
Compressive Fracture Energy, G_c (N.m/m ²)	20,00	10 mm deformed bars	450
	0		650



(a) Final damage in specimen 4

(b) Finite element mesh used in the simulations

Fig. 9 Specimen 4 of Mehrabi *et al.* (1994)

The ability of the numerical model to simulate the progressive damage on the reinforced concrete frame and the URM infill wall members and predict the final mode of failure were also investigated. For the four points circled on the pushover curve of Specimen 4 in Fig. 10, vectors of in-plane principal compressive stresses, crack patterns (disc plots of crack strains in DIANA 2008) and shear force distribution along boundary columns are given in Table 3.

The principal stress vectors help the visualization of the load path within the URM infill wall (Table 3). The formation of the compression strut mechanism can openly be observed as the lateral displacement increased. Crack strain plots provide the visual representation of crack patterns in the URM infill wall and the RC frame members. The crack directions indicate the normal direction to the principle tensile strain direction, which was assumed to be the same as the principle tensile stress direction in the material model. The final damage pattern observed for Specimen 4 tested by Mehrabi *et al.* (1994) is given in Fig. 9. The simulation results presented in Table 3 seem to indicate a reasonable agreement between model predictions and the experimental observations. The simulated failure occurred in the URM infill wall with inclined shear cracks extending into columns were similar to those observed in the experiment. Flexural crack pattern estimations of the analysis were also in good agreement with the observed damage.

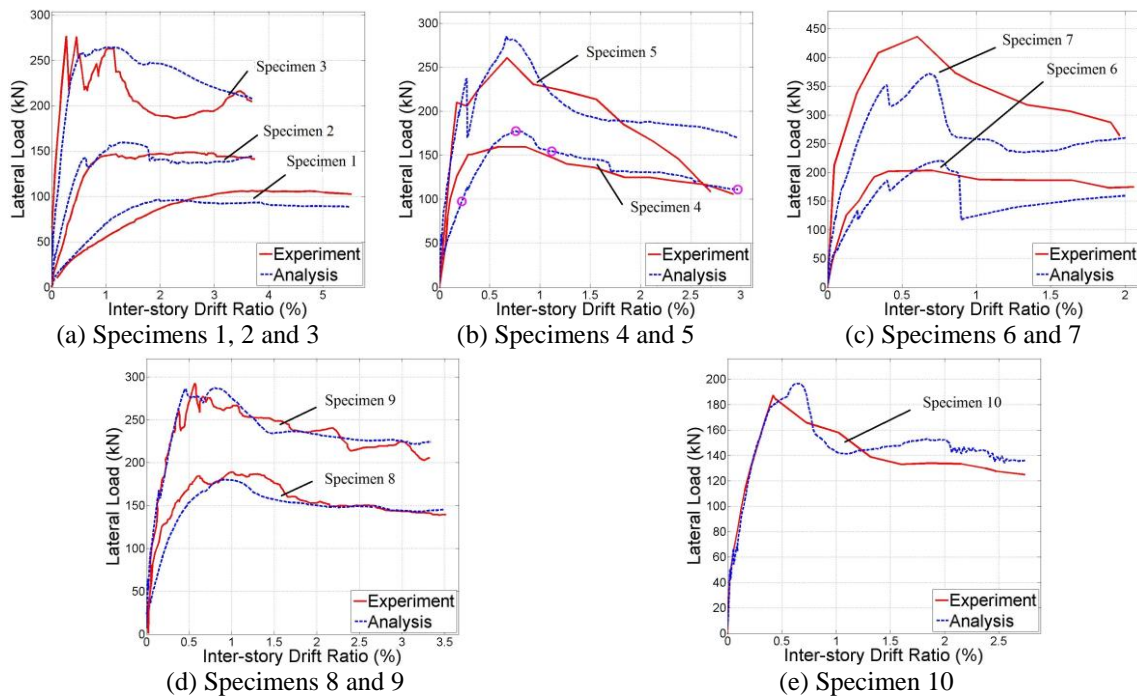


Fig. 10 Results of the pushover analyses

Shear force diagrams of the boundary columns were obtained by post-processing the stresses. Results show that because of the compressive strut action developing in the URM infill wall, considerable amount of shear force was transferred to the column end zones. However, due to the weak URM infill wall material and relatively strong bounding frames, the strut capacity was exhausted before the full shear capacity of the columns was reached. This resulted in a relatively ductile response for the considered frame. Captive column formation was observed after the first

diagonal crack formation in the infill wall. The resulting shear, however, did not exceed the shear capacity of the column, but caused extensive cracking within the captive zone. This observation can be justified with the observed damage pattern in the experiment (Fig. 9).

3.3 Dynamic analysis of the test frame

Results of the simulations presented in the previous section provided sufficient confidence on the accuracy of the modeling approach. Consecutive nonlinear time history analyses of the test frame for the three ground motions (Fig. 4) were conducted using previously described FE modeling scheme shown in Fig. 7. A damping ratio of 2% was used in the analysis. An implicit Newmark-Beta time integration method was used for the solution of the system of equations in the dynamic analysis. The objective of the analysis was to observe the ability of estimating the dynamic response of the test frame and to further elaborate on the force distributions on boundary columns.


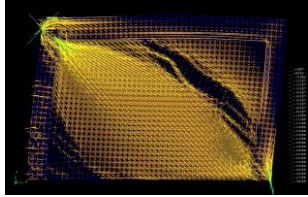
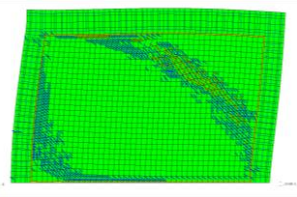
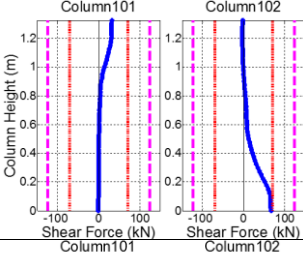
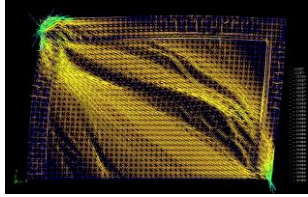
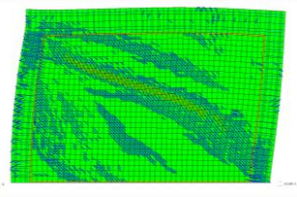
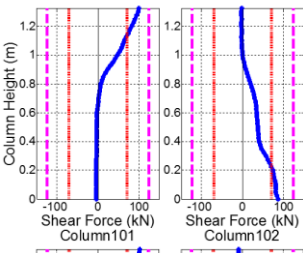
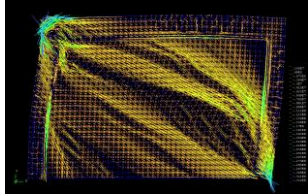
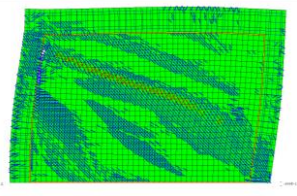
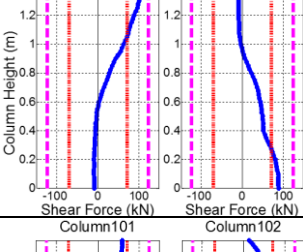
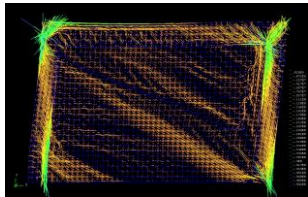
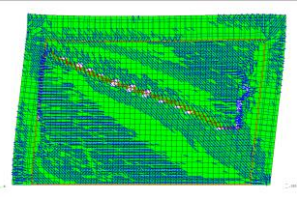
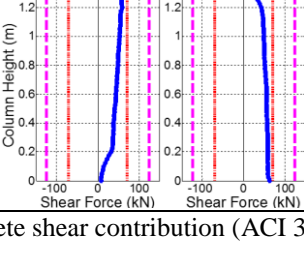
Interstory drift ratio time history comparisons of experimental and analytical results for each floor are given in Fig. 11. The agreement of time series between numerical and experimental results is reasonable. Shear force versus interstory drift ratio estimations for each story from time history analyses are presented along with the experimental results in Fig. 12. It is observed that the numerical simulation results underestimated the first story interstory drifts and overestimated the interstory drifts of the second and the third story. The lateral strength of the frame was overestimated by about 15% in one direction and 10% in the other. For the last ground motion, the finite element model failed to capture the period elongation due to the high inelastic action and stiffness degradation (Fig. 11). It can also be observed that the initial stiffness of the system was estimated accurately. However, the pinching behavior, which was observed in the experiment, cannot be observed in the simulation results. This was mainly due to the limitations of the material models with secant unloading and absence of any bond-slip model for the reinforcement, which could not mimic the very complex nonlinear cyclic behavior with a continuum approach.

In addition to the global response parameters such as story shear forces and interstory drift ratios, local responses such as member-end strains and rotations for the first story columns were also compared. Numerical simulation results revealed that strain and rotation predictions for bottom end of the first story columns was also in good agreement with the experimental results, showing similar trends as the global parameters (Fig. 13). However, the top end rotations were not estimated with adequate accuracy as bottom end rotations (Fig. 14). The model was successful in estimating the rotations at the fixed base; however, it failed to simulate the rotations of the top ends where a more complex stress state was present due to the flexible joints. The average strain measurements measured along the infill wall diagonal was also compared with the analysis results (Fig. 15). The measured peak diagonal strain of about 1% was predicted closely with the numerical simulations. However, the damping in the experiments, causing the decay of strain amplitudes more rapidly beyond the peak strain, was more pronounced compared to the simulation results.

Numerical simulations of the same tests were also conducted by Boljevic (2015) using the equivalent diagonal strut approach with Opensees platform. In his study, two different strut models were employed. Simulations using the strut model by TEC (2007) gave unacceptably large errors when compared with the experimental results. Better estimation of shear force and interstory drift ratio (20% and 30% error in maximum values, respectively) were obtained using the method proposed by Dolsek and Fajfar (2002) where the hysteretic behavior of the strut is obtained from the difference of experimental results of the bare and infilled frames with same properties. From the results of Boljevic (2015) it can be concluded that story shear comparison showed better matching

of analytical and experimental results than story drift comparison. Furthermore, additional distributed forces and their distribution on the boundary columns could not be obtained with the equivalent diagonal strut approach.

Table 3 Progression of damage and member force distributions during pushover analysis

Roof Disp.	In-plane Compressive Stress Vectors	Crack Patterns	Shear Force Diagrams of Columns*		Comments
3 mm (1)					Initial cracks at the infill, Diagonal compressive strut formation, shear transferred to boundary columns
10 mm (2)					First diagonal crack occurs in URM infill, off-diagonal strut formation, progression of shear transfer, shear damage in columns.
15 mm (3)					Increased damage in URM infill, partial failure of strut mechanism, flexural cracking in RC members due to increased drift
40 mm (1)					Crushing of the infill, failure of strut mechanism, negligible shear transfer due to infill, further flexural cracking in RC members

* V_n : nominal shear strength (ACI 318-11 2011), V_c : concrete shear contribution (ACI 318-11 2011)

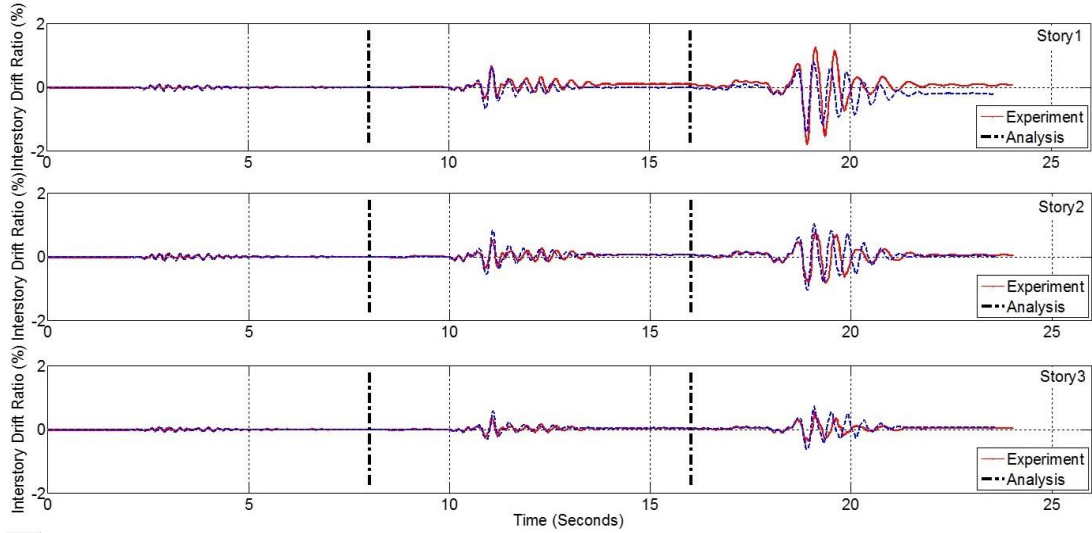


Fig. 11 Interstory drift ratio history comparison

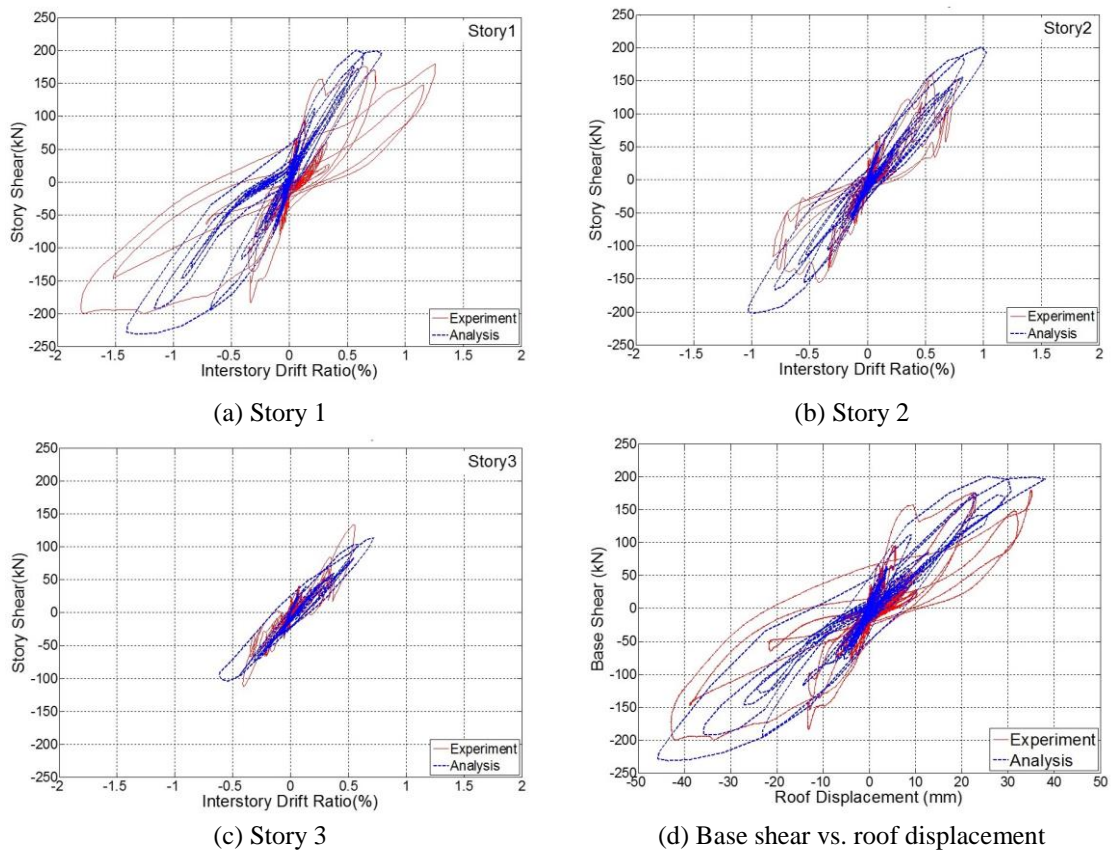


Fig. 12 Force- deformation response comparison

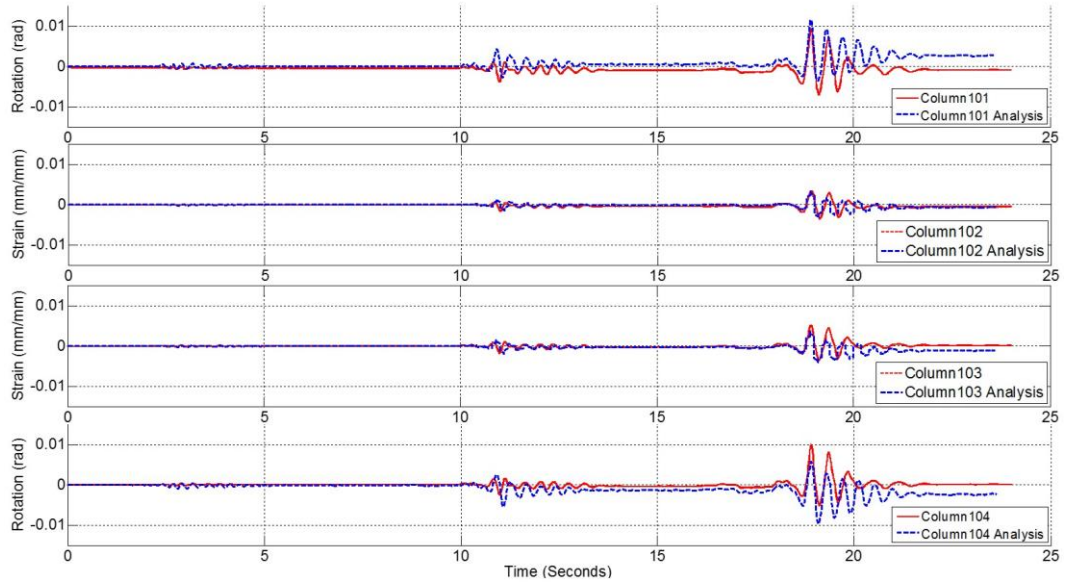


Fig. 13 Local responses at the bottom the of first story columns

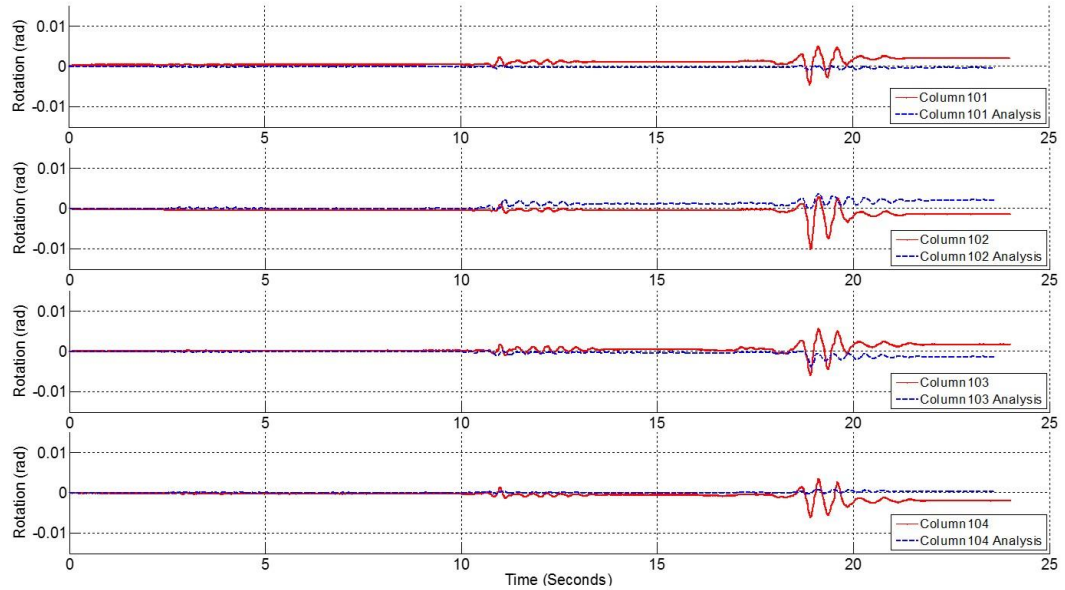


Fig. 14 Local responses at the top of first story columns

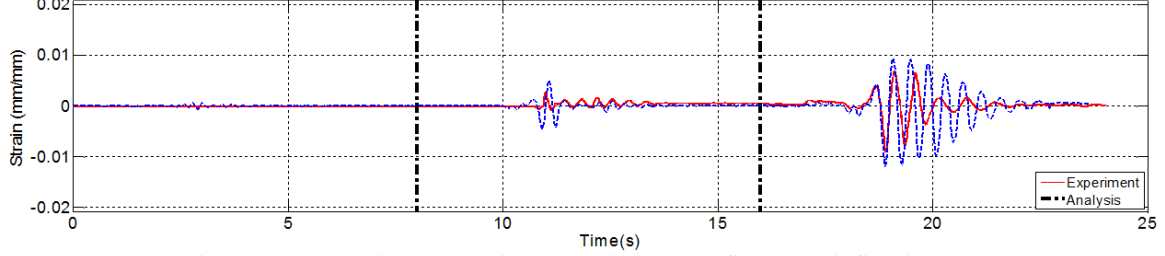


Fig. 15 Average diagonal strain comparison at the first story infill diagonal

4. Performance assessment

Using the numerical simulation results, crack patterns of the first story infill wall and its adjacent columns were obtained at the peak roof displacement and compared with the final damage observed in the experiment (Fig. 16). Crack patterns (only open cracks are shown in Fig. 16) showed good agreement between experimental and simulation results. From the damage pattern of the experiment, inclined cracks were observed along a distance up to half of the column length from the member ends, revealing the compression strut width. ASCE-SEI 41-06 estimation of the strut width, on the other hand, was calculated as 0.25 m using

$$a = 0.175(\lambda_1 h_{col})^{-0.4} r_{rinf} \quad (3)$$

where

$$\lambda_1 = \left[E_{me} \frac{t_{inf} \sin 2\theta}{4E_{fe} I_{col} h_{inf}} \right]^{\frac{1}{4}} \quad (4)$$

In above equations, a stands for the strut width, h_{col} for the column height, r_{rinf} for the diagonal length of the infill panel, t_{inf} for the thickness of the infill wall and h_{inf} for the height of the infill. E_{me} and E_{fe} represent the elastic modulus of masonry infill wall and frame materials respectively and I_{col} represents the moment of inertia of the column section in its bending direction. θ is the angle whose tangent is the infill wall height to length aspect ratio (Fig. 1).

To further elaborate on the shear force variation along the boundary and isolated columns, shear diagrams of the first story columns were obtained (Fig. 17) by integrating the shear stresses. Shear capacities of the columns were also calculated according to ACI 318-11 (2011), including axial load effects and plotted along with the shear diagrams. It can be observed that for the exterior columns, shear force demand was constant and below the calculated shear strength. On the other hand, shear force demand was found to linearly vary along a certain portion of the boundary columns, implying that the force is transferred from the infill wall to the boundary columns in the form of a nearly uniformly distributed load. As mentioned in section 1, the shear force demand at the boundary column can be calculated with two methods in ASCE/SEI 41-06. The horizontal component of the strut force was estimated for columns 102 and 103 using:

$$V_{inf} = f_m A_{inf} \quad (5)$$

where A_{inf} is the area of net mortared/grouted section in the infill wall and f_m is the masonry shear strength. The calculated shear demand was found to be much smaller (37.2 kN) compared to the computed shear force demand from numerical simulations. On the other hand, the shear demand was also calculated considering a possible captive column induced shear demand using:

$$V = \frac{2M_{pc}}{L_{eff}}, \quad L_{eff} = a/\cos\theta \quad (6)$$

where M_{pc} indicates the plastic moment capacity of the column, L_{eff} is the effective column length, a is the strut width. The angle θ was already shown on the wall geometry (Fig. 1). Here, a and θ should be calculated according to Eqs. (3) and (4). From the point of estimating a possible captive column induced shear demand, ASCE/SEI 41-06 gave a conservative estimation (171 kN). However, it should be mentioned that, a captive column situation was not observed during the test, which would justify the choice of estimation based on Equation 5. However, this estimation is on the unsafe side for the estimation of forces transferred on the boundary columns. The two results obtained using ASCE/SEI 41-06 guidelines are found to be inconsistent and which result to be used is not clearly stated by the document.

Another point, which requires attention is during the experiment, inclined cracks beyond the column confinement length were observed. Simulation results also showed that there exist significant shear forces beyond the confinement region of boundary columns (Fig. 17). Extensive shear damage observed in the boundary columns during the experiment, revealed that although the shear design of the boundary columns was conducted according to the capacity design principles for a bare frame, shear damage would occur in parallel with the visual observations. This result shows that the boundary columns are prone to shear failures and they can no longer be classified as ductile members when design is conducted according to TEC (2007). In the code, design for higher forces are enforced if the required ductility cannot be ensured. The designer can only ensure ductile response by considering the additional shear forces transferred from the infill wall to the boundary columns through more stringent transverse reinforcement detailing.

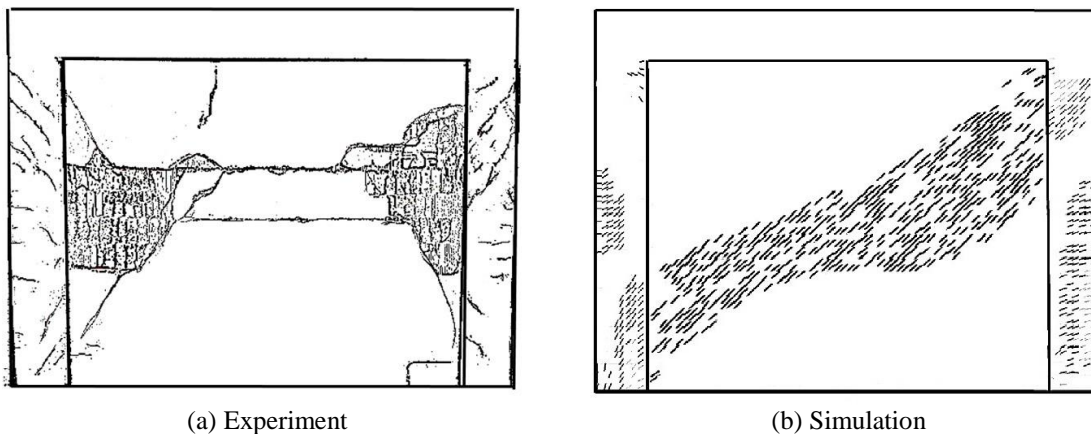


Fig. 16 Crack patterns

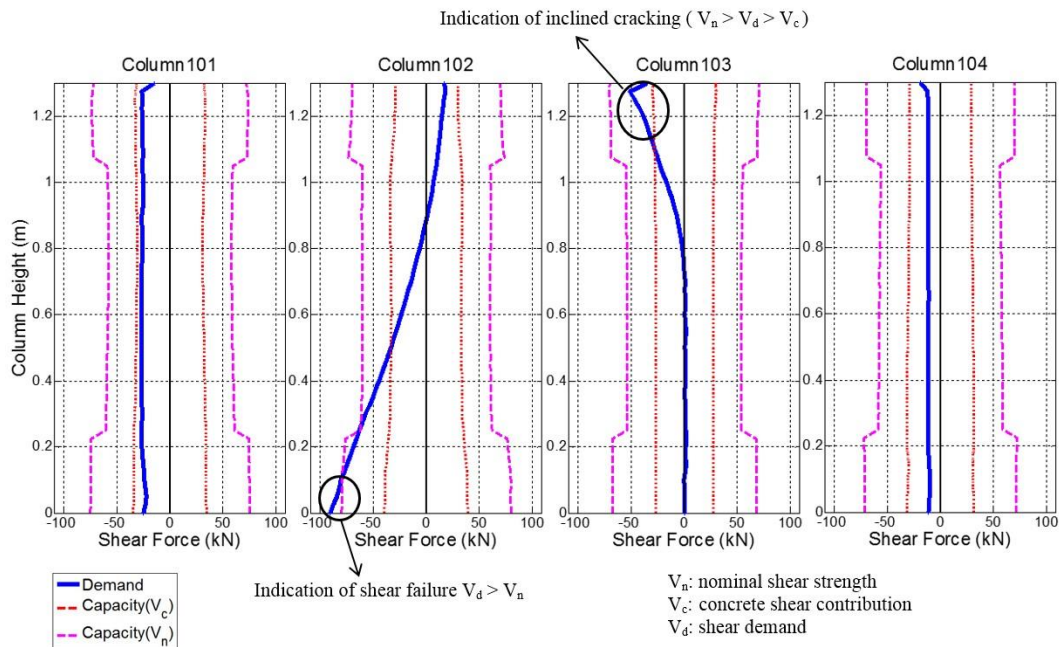


Fig. 17 Shear force diagrams of first story columns at peak deformation

Seismic assessment of the test specimen was carried out according to ASCE/SEI 41-06 (2006) guidelines including the updates presented by Elwood *et al.* (2007). For the RC buildings with URM infill walls, modeling parameters and acceptance criteria of boundary columns differ from those used for regular columns. For reinforced concrete columns, modeling parameters and acceptance criteria are defined in terms of plastic rotations whereas they are defined in terms of total average strain for the boundary columns as discussed in Section 1. The previously mentioned numerical model was used for the seismic assessment. Assessment of all the column members except boundary columns were conducted using the plastic rotation based approach of ASCE/SEI 41-06. On the other hand, the columns adjacent to the infill walls in the central bay were evaluated according to the strain based numerical acceptance criteria given by ASCE/SEI 41-06. The assessment of infill walls were made by using the drift based procedure of ASCE/SEI 41-06.

Observed damage of the first story columns and the first story infill wall at the end of the D4 earthquake are given in Fig. 18. The performance levels corresponding to the observed damage of members were determined using the criteria given in ASCE/SEI 41-06. The boundary columns had major shear cracks, which led the authors to judge the damage state as limited safety (between Life Safety and Collapse Prevention) based on visual observation. On the other hand, exterior columns did not have any shear cracks and had only minor cover spalling. This observed damage was considered to satisfy the life safety performance level and therefore the specimen was called to be in the damage control performance range (between Immediate Occupancy and Life Safety). The observed damage in the first story infill wall indicated Limited Safety performance level due to spalling of masonry blocks and large see-through cracks where the second and third story walls had only minor cracks and was judged to be Immediate Occupancy level.

Performance assessment results obtained by using ASCE/SEI 41-06 are shown in Fig. 19. Fig. 20 presents the plastic hinge rotation limits for columns along with the demands. The average axial strain limits of ASCE/SEI 41-06 in the boundary columns and the numerical results considering the

strains along the full height and within the plastic hinge region are also provided in the same figure. The limiting interstory drift ratio value for the Life Safety performance level, which is the only available performance limit for the infill walls, was 0.86 percent from ASCE/SEI 41-06. This value was used for the assessment of infill walls according to ASCE/SEI 41-06.

The plastic rotation based procedure concerning the exterior columns gave accurate estimations of the actual damage state observed in the test. In the case of boundary columns, however, when the average axial strain along the entire length of the member was considered, the strain limits provided by the guidelines seemed to be much higher than the calculated strain demands. The main reason of this situation was the averaging of the axial strains along the column height, which were in fact concentrated within the column ends. Hence, the use of average axial strains for boundary columns resulted in unsafe estimations of the damage. Although the infill wall damage at the first story was estimated correctly, the URM infill wall damage in the upper stories was significantly overestimated.

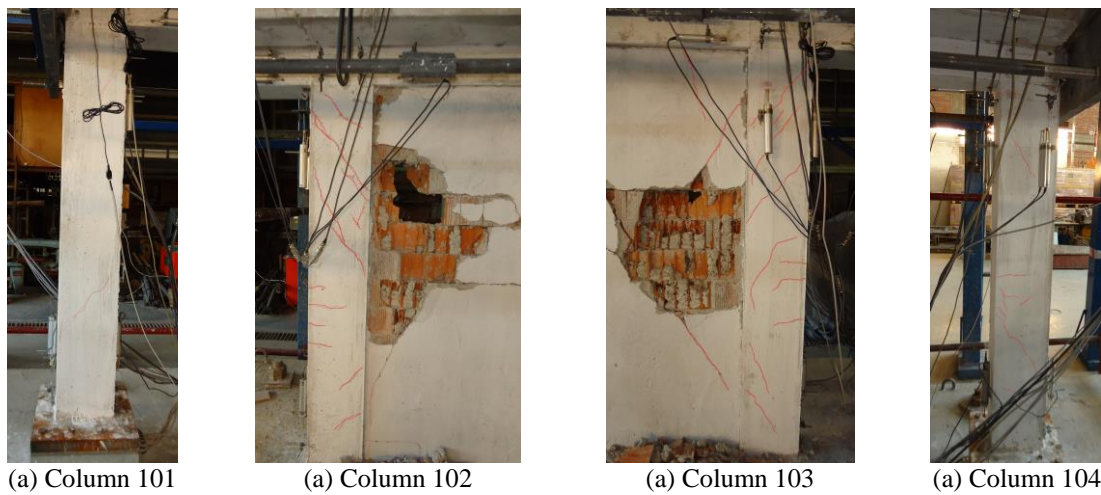


Fig. 18 Observed damage at the end of the experiment

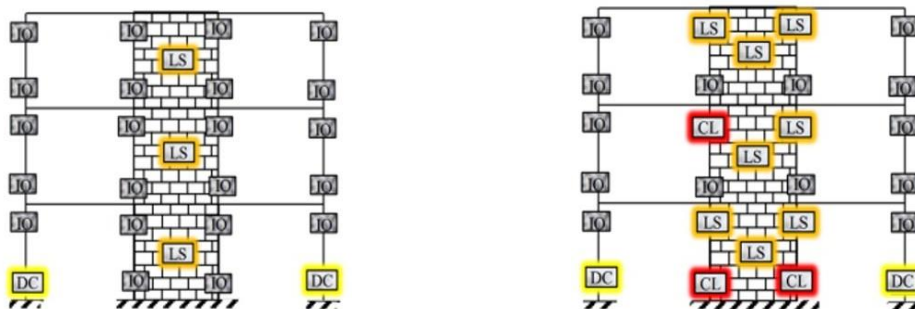
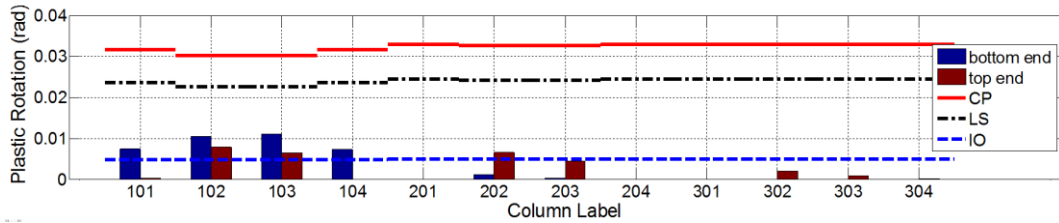
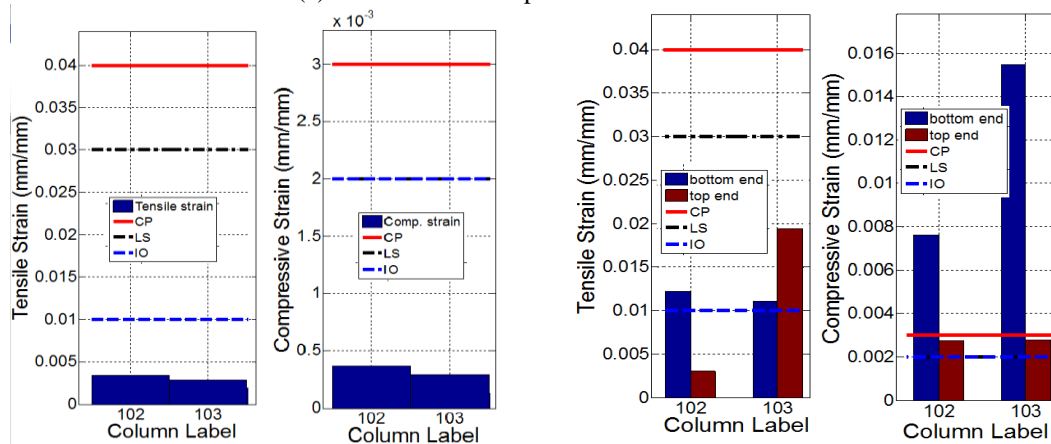


Fig. 19 Seismic assessment of columns (IO: immediate occupancy, DC: damage control, LS: limited safety, CL: collapse)



(a) ASCE/SEI 41-06 plastic rotation based method



(b) ASCE/SEI 41-06 approach

(c) Using total strain in plastic hinge region

Fig. 20 Numerical results of seismic assessment of boundary columns

As an alternative to the existing approach given by ASCE/SEI 41-06, assessment of boundary columns was conducted using strain demand as the total average strain within the plastic hinge zone (i.e. half-length of the column depth from column top and bottom, TEC 2007). In this approach, strain limits given in the ASCE/SEI 41-06 document was used as given in Table 1 without any modification. Assessment results for both approaches are given in Fig. 19 and 20. It should be noted that the strains in the plastic hinge region of the columns were in good agreement with the experimental results (Fig. 13), implying the assessment results are the same if the experimental data was used. As it can be seen in this figure, the use of plastic hinge strains at the boundary column ends yielded better estimations of the damage level. Although the estimated damage levels are still slightly on the conservative side, the modified approach gives better prediction of the expected damage of the boundary column assessment.

5. A simple proposal

For the performance assessment of existing RC buildings with URM infill walls, a simple methodology can be devised in the light of existing guidelines (ASCE/SEI 41-06 2006, Eurocode 8 2004 and TEC 2007) and aforementioned results. The shear force demand on the boundary columns depend on the expected failure mode of the infill wall and interstory drift ratio demand. The ultimate interstory drift ratio for infill walls was studied by Turgay *et al.* (2014) in light of a database of 50 tests from the literature (Fig. 21). In the figure, the line marked as average refers to average drift limit obtained from experiments where the line marked as proposed refers to the proposed drift limit. Based on these results, a drift ratio limit of 0.5 to 0.75 percent can be selected as a lower bound limit

for infill wall deformability. If the interstory drift ratio demand is smaller than this limit, then it may be assumed that infill wall continues to transfer the lateral force by forming a compression strut without any significant strength degradation. For this case, the boundary columns should be checked for the additional shear force transferred from the lateral component of the compression strut force. Conversely, if the drift ratio limit is exceeded, then the infill wall is expected to sustain significant damage. Among the failure modes observed in the tests shown Fig. 21, corner crushing appears to be the most critical mode as it leads to formation of a captive column. The shear force resulting from the captive column formation can then be calculated using Equation 6.

For both cases, depending on the column shear force demand to capacity ratio and transverse steel reinforcement details, column classification can be made similar to conventional columns and the assessment can be conducted with the existing performance limits. However, use of plastic hinge strains instead of average strains along the column length is recommended (Fig. 19 and 20).

The aforementioned procedure can also be employed for new design. If the interstory drift demand is smaller than the limit mentioned above, the transverse reinforcement of the column can be designed by considering the lateral force transferred from the lateral component of the compression strut force. On the other hand, if the interstory drift demand is larger than the deformation limit of the infill wall, corner crushing will be the critical mode and the transverse reinforcement of the column should be detailed for the shear force considering the captive column formation according to Equation 6.

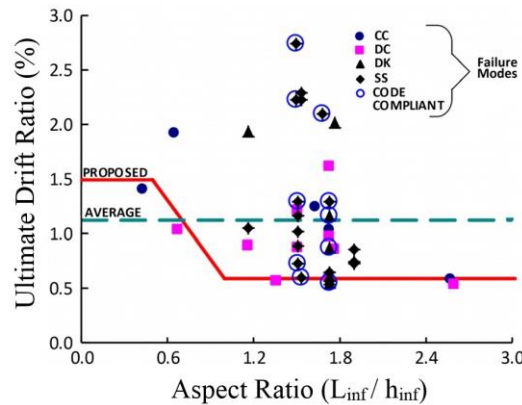


Fig. 21 Ultimate Deformation Capacity of Infilled Frames (CC: corner crushing, DC: diagonal cracking, DK: diagonal compression, SS: sliding shear)

6. Conclusion

Experimental, numerical simulation and seismic assessment results are presented for the considered test frame. The following conclusions are extracted in light of the experimental and analytical study:

- The seismic behavior of reinforced concrete frames is significantly altered by the presence of infill walls. Stiffness, strength, deformation capacity, and ductility of such structures are affected greatly by the frame-infill wall interaction. Substantial amount of shear force is transferred from infill walls to the boundary columns in the form of a uniform distributed load along the strut width. This results in shear damage on boundary column members and prevents the ductile behavior if the column was not designed for such forces.

- Global demand parameters such as interstory drift ratios and base shear capacity are estimated with adequate accuracy using fairly sophisticated methods available to the engineers in practice. Continuum modeling of the infill wall was found to be satisfactory in terms of estimating the global behavior and the shear damage on boundary columns. However, local demand parameters were found difficult to estimate even with continuum modeling.
- Guidelines provided by ASCE/SEI 41-06 exhibited accurate estimations regarding exterior columns, however the strain based method provided for the assessment of boundary columns were found to be unsafe and lacking accuracy for the considered test frame. When the strain limits were considered for plastic hinge strains at the member-ends, procedure gave better estimations remaining on the conservative side. The observed failure mode did not indicate a captive column formation and the estimated shear force to be transferred on the column based on a sliding shear mechanism was on the unsafe side according to ASCE/SEI 41. This finding reveals that the approach of shear force estimation method of ASCE/SEI 41 lacks consistency with the test observations.
- For the assessment of existing buildings, a simple method was proposed to take into account the influence of forces transferred from the infill walls to the boundary columns.
- The boundary columns should be designed for the additional shear forces transferred from the infill wall. To calculate the design shear force, the same methodology proposed for the assessment can be applied.

Acknowledgements

The research described in this paper was financially supported by TUBITAK Project No: 108G034. Second author acknowledges the support provided by TUBA-GEBIP program.

References

- ACI 318-11 (2011), "Building code requirements for structural concrete", *American Concrete Institute*, Detroit, Michigan, USA.
- ASCE/SEI 41-06 (2006), "Seismic rehabilitation of existing buildings", *American Society of Civil Engineers*, Reston, Virginia, USA.
- Bertero, V.V. and Brokken, S. (1983), "Infills in seismic resistant building", *J. Struct. Eng (ASCE)*, **109**(6): 1337-1361.
- Binici, B., Canbay, E., Ozcebe, G., Yakut, A., Aldemir, A., Demirel, I.O., Erdil, B., Kale, O. (2012), "Observations regarding seismic and structural damage for november 9th 2011 M_w 5.6 Van-Edremit earthquake", *METU-EERC Rep. No. 2012-1*, Turkish Chamber of Civil Engineers, Ankara, Turkey.
- Boljevic, B. (2015), "An assessment of the strut models for seismic analysis of infilled frames", Ph.D. Dissertation, Middle East Technical University, Ankara, Turkey.
- Canbay, E., Ersoy, U., Tankut, T. (2004), "A three-component force transducer for RC structural testing", *Engineering Structures*, **26**(2):257-265.
- Dolsek, M., Fajfar, P. (2002), "Mathematical modeling of an infilled RC frame structure based on the results of pseudo-dynamic tests", *Earthquake Engineering and Structural Dynamics*, **31**:1215-1230.
- DIANA (2008), "Displacement analyses user's manual", *TNO DIANA*, Delft, Netherlands.
- El-Dakhkhni, W., Elgaaly, M., Hamid, A.A. (2003), "Three-strut model for concrete masonry-infilled steel frames", *J. Struct. Eng (ASCE)*, **129**(2):177-185.

- Elwood, K.J., Matamoros, A.B., Wallace, J.W., Lehman, D.W., Heintz, J.A., Mitchell, A.D., Moore, M.A., Valley, M.T., Lowes, L.N., Comartin, C.D., Moehle, J.P. (2007), "Update to ASCE/SEI 41 concrete provisions", *Earthquake Spectra*, **23**(3): 493-523.
- Erdik, M. (2000), "Report on 1999 Kocaeli and Duzce (Turkey) earthquakes", *Proc. of the 3rd Intl. Workshop on Structural Control*, Paris, 149-186.
- Eurocode 8 (2004), "Design of structures for earthquake resistance—part 1: general rules, seismic actions and rules for buildings", CEN: Brussels, Belgium.
- Fardis, M.N., Bousias, S.N., Franchioni, G., Panagiotakos, T.B. (1999), "Seismic response and design of RC structures with plan-eccentric masonry infills", *Earthq. Eng. Struct. Dyn.*, **28**(2):173-191.
- Favvava, J.F., Naoum M.C., Karayannis, C.G. (2013), "Limit states of RC structures with first floor irregularities", *Structural Engineering & Mechanics*, **47**(6):791-818.
- Feenstra, P.H. (1993), "Computational aspects of biaxial stress in plain and reinforced concrete", Ph.D. Dissertation, Delft University of Technology, Delft, Netherlands.
- Fiorato, A.E., Sozen, M.A., Gamble, W.L. (1970), "An investigation of the interaction of reinforced concrete frames with masonry filler walls", *Civil Eng. Studies, Structural Research Series Rep. No.370*, Univ. of Illinois, Urbana-Champaign IL, USA.
- Hashemi, A., Mosalam, K.M. (2007), "Seismic evaluation of reinforced concrete buildings including effects of masonry infill walls", PEER Technical Report 2007/100.
- Kakaletsis, D.J., Karayannis, C.G. (2007), "Experimental investigation of infilled RC frames with eccentric openings", *J. Structural Engineering Mechanics (SEM)*, **26**(3):231-250.
- Kakaletsis, D.J., Karayannis, C.G. (2009), "Experimental Investigation of infill RC frames with openings", *ACI Structural J.* **106**(2): 132-141.
- Klinger, R.E. and Bertero, V.V. (1976), "Infilled frames in earthquake-resistant construction", Report EERC/76-32. Earthquake Engineering Research Center, University of California, Berkeley, CA, USA.
- Kurt, E.G., Binici, B., Kurç, Ö., Canbay, E., Akpınar, U., Ozcebe, G. (2011), "Seismic performance of a deficient reinforced concrete test frame with infill walls", *Earthquake Spectra*, **27**(3): 817-834.
- Mainstone, R.J. (1971), "On the stiffness and strength of infilled frames", *Proc. Trans. Institute of Civil Engineers Suppl. IV*, Institute of Civil Engineers, London, England.
- Marjani, F. (1997), "Behavior of brick infilled reinforced concrete frames under reversed cycling loading", Ph.D. Dissertation, Middle East Technical University, Ankara, Turkey.
- Mehrabi, A.B., Shing, P.B., Schuller, M.P., Noland, J.L. (1994), "Performance of masonry-infilled R/C frames under in-plane lateral loads", *Structural Engineering and Structural Mechanics Research Series*, University of Colorado at Boulder, Dept. of Civil Envir. and Arch. Engineering, Colorado, USA.
- Mehrabi, A., Shing, P. (1997), "Finite Element Modeling of Masonry-Infilled RC Frames." *J. Struct. Eng (ASCE)* **123**(5): 604–613.
- Molina, F.J., Verzeletti, G., Magonette, G., Buchet, P.H., Gérardin, M. (1999a), "Bi-directional pseudodynamic test of a full-size three-storey building", *Earthq. Eng. Struct. Dyn.*, **28**(12):1541-1566.
- Molina, F.J., Verzeletti, G., Magonette, G., Buchet, P.H., Gérardin, M. (1999a), "Bi-directional pseudodynamic test of a full-size three-storey building", *Earthq. Eng. Struct. Dyn.*, **28**(12):1541-1566.
- Molina, F.J., Pegon, P., Verzeletti, G. (1999b), "Time-domain identification from seismic pseudodynamic test results on civil engineering specimens", *Proceedings of 2nd International Conference on Identification in Engineering Systems*, University of Wales, Swansea, Wales.
- Mosalam, K.M., White, R.N., Ayala, G. (1998), "Response of infilled frames using pseudo-dynamic experimentation", *Earthq. Eng. Struct. Dyn.*, **27**(6):589-608.
- Selby, R.G. and Vecchio, F.J. (1993), "Three dimensional constitutive relations for reinforced concrete", *Technical Report No. 93-02*, Department of Civil Engineering, University of Toronto, Toronto, Canada.
- Stavridis, A. and Shing, P.B. (2010), "Finite-element modeling of nonlinear behavior of masonry-infilled RC frames", *J. Struct. Eng (ASCE)*, **136**(3):285–296.
- Sucuoglu, H., Binici, B., Canbay, E., Kurç, O., Ozcebe, G. (2013), "A study towards development of new generation performance based codes, 108G084 Tubitak Final Report, Ankara, Turkey.

- TEC (2007), “Turkish code for buildings in seismic zones”, *Ministry of Public Works and Settlement*, Ankara, Turkey (In Turkish).
- Turgay, T, Durmus, M.C., Binici, B., Ozcebe, G. (2014), “Evaluation of the predictive models for stiffness, strength, and deformation capacity of RC frames with masonry infill walls”, *J. Struct. Eng (ASCE)*, **140**(10).
- Vecchio, F.J. and Collins M.P. (1993), “Compression response of cracked reinforced concrete”, *J. Struct. Eng (ASCE)*, **119**(12): 3590-3610.
- Van Noort, J.R. (2012), “Computational modeling of masonry structures”, Master Thesis, Delft University of Technology, Delft, Netherlands.